PAPER

Multi-nuclear, high-pressure, *operando* FlowNMR spectroscopic study of Rh/PPh₃ — catalysed hydroformylation of 1-hexene†

Alejandro Bara-Estaún, [ID] ab Catherine L. Lyall, [ID] ab John P. Lowe,ab Paul G. Pringle, [ID] d Paul C. J. Kamer, [ID] e Robert Frankef and Ulrich Hintermair [ID] *abc

The hydroformylation of 1-hexene with 12 bar of 1 : 1 H_2/CO in the presence of the catalytic system [Rh(acac)(CO)$_2$]/PPh$_3$ was successfully studied by real-time multinuclear high-resolution FlowNMR spectroscopy at 50 °C. Quantitative reaction progress curves that yield rates as well as chemo- and regioselectivities have been obtained with varying P/Rh loadings. Dissolved H_2 can be monitored in solution to ensure true *operando* conditions without gas limitation. ^{31}P{^{1}H} and selective excitation ^{1}H pulse sequences have been periodically interleaved with ^{1}H FlowNMR measurements to detect Rh–phosphine intermediates during the catalysis. Stopped-flow experiments in combination with diffusion measurements and 2D heteronuclear correlation experiments showed the known tris-phosphine complex [RhH(CO)(PPh$_3$)$_3$] to generate rapidly exchanging isomers of the bis-phosphine complex [Rh(CO)$_2$(PPh$_3$)$_2$] under CO pressure that directly enter the catalytic cycle. A new mono-phosphine acyl complex has been identified as an in-cycle reaction intermediate.

Introduction

Hydroformylation, also known as the "oxo process", reacts olefins with a mixture of CO and H_2 ("syngas") to yield aldehydes in the presence of a suitable catalyst.[1] With terminal alkenes (α-olefins), the proportions of linear *n*-aldehydes and branched iso-aldehydes formed are a measure of the regioselectivity of the catalyst (Fig. 1).

aDepartment of Chemistry, University of Bath, Claverton Down, BA2 7AY Bath, UK. E-mail: u.hintermair@bath.ac.uk

bDynamic Reaction Monitoring Facility, University of Bath, Claverton Down, BA2 7AY Bath, UK
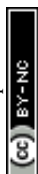
cCentre for Sustainable & Circular Technologies, University of Bath, Bath BA2 7AY, UK
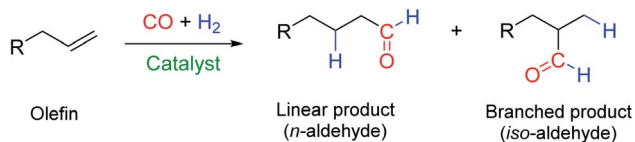
dSchool of Chemistry, University of Bristol, Cantock's Close, Bristol BS8 1TS, UK

eLeibniz Institute for Catalysis, Albert-Einstein-Straße 29A, 18059 Rostock, Germany

*fEvonik Performance Materials GmbH, Paul-Baumann-Straße 1, 45772 Marl, Germany*

Fig. 1   General chemical equation of a hydroformylation reaction.

Chemoselectivity towards aldehyde formation is also important in the process as many catalysts also produce internal olefins (isomerization of α-olefins), paraffins (hydrogenation of olefins) and alcohols (hydrogenation of aldehydes) to various degrees.[2]

Otto (Roelen) discovered the hydroformylation of olefins in 1938 following its initial observation as a side reaction in Fischer–Tropsch chemistry.[3] Hydroformylation has since undergone rapid development to become one of the largest industrial homogeneously catalysed processes, as well as an important academic research field with a large number of papers and patents from all over the world.[2] Although rarely used for chemical synthesis on small scale,[4] hydroformylation is frequently employed as a benchmark reaction for new ligands due the intricate interplay of chemo-, regio- and enantio-selectivity of the reaction.[5] Although Ir, Ru and Fe based hydroformylation catalysts are known, Rh and Co complexes still stand out due to their superior activity, especially on an industrial scale.[6] Co-based catalysts are tolerant toward trace impurities in the alkene feedstock, but require relatively harsh reaction conditions (>150 °C and >100 bar syngas) and display significant hydrogenation activity. The latter is often exploited to directly produce alcohols,[7] albeit accompanied by significant paraffin co-production and formation of heavy aldol condensation side-products. Rh-based catalysts are generally more active and more selective than Co catalysts and operate under milder conditions (<100 °C and <50 bar syngas) but Rh is decisively more expensive due its rarity and widespread use in the automotive industry.[8] Nevertheless, its higher efficiency explains why over 80% of all hydroformylation plants built after 1985 utilize Rh catalysts.[9] In 2008, the global production of oxo compounds was about 10.4 million metric tons, and many large-scale plants manufacture several hundred thousand metric tons per year.[10] Linear aldehydes are the main product as they are target intermediates for subsequent bulk chemical production of esters, alcohols and amines, while branched aldehydes are mostly desired for fine chemical production, partly due to the generation of
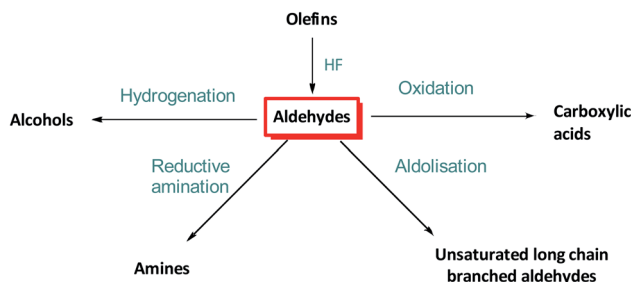
Fig. 2   Industrial uses of aldehydes generated by olefin hydroformylation.[2]

a stereogenic centre at the formylated secondary carbon (Fig. 2).[11,12] Long chain α-olefin substrates are usually synthesised by oligomerization of ethylene,[13] whereas styrene and related molecules are preferred for asymmetric hydroformylation for fine chemical production.[14,15]

Many organometallic Rh species have been investigated with a large variety of mono- and bidentate phosphorus ligands such as phosphites and phosphines.[16–19] The identity of the ligand is crucial as they can tune, through their electronic and steric properties, the activity, regioselectivity, chemoselectivity and enantioselectivity of the hydroformylation reaction.[20,21] The first mechanistic study of this reaction using $[RhH(CO)(PPh_3)_3]$ as the precursor was carried out over 50 years ago by Wilkinson[22] who proposed a mechanism for the olefin hydroformylation that is still accepted as conceptually correct. Since then many studies with a variety of reaction conditions, ligands and metals have been performed, both experimentally and computationally.[16,23–26] Despite the large number of publications in which different mechanisms are proposed, several of the suggested intermediate species have never been observed. The difficulty of studying this reaction under working conditions is due to the high syngas pressure and temperatures employed, in addition to the O_2 sensitivity of the Rh catalyst.[27] A combination of kinetic studies, *in situ* IR investigations and high-pressure ^{31}P NMR studies in static sapphire tubes have contributed much to this field.[28,29] However, very few *operando* studies (*in situ* measurements during catalytic turnover) have been performed to verify mechanistic hypotheses and understand the electronic and steric parameters of the ligands and any other conditions that may affect the catalytic performance. Van Leeuwen, Kamer and co-workers have developed bespoke high-pressure infrared spectroscopy (HP-IR) autoclaves that allow *operando* IR studies of fast catalytic reactions under realistic conditions,[24] and other groups have used similar setups to follow Rh-catalysed hydroformylation on different scales.[30,31] IR spectroscopy offers high sensitivity and fast measurements compared to NMR spectroscopy, but it requires calibration to be quantitative and provides limited structural information on the intermediates observed.[32] On-line high resolution FlowNMR spectroscopy has recently been shown to be a powerful *operando* reaction monitoring technique for homogeneous catalytic systems under realistic conditions due to its quantitative nature and high specificity in complex reaction mixtures.[33] A recent report includes an example of an *operando* investigation of Rh/phosphite-catalysed hydroformylation using FlowNMR but with a limited amount of data and experimental details.[34] Landis recently reported a detailed kinetic study of Rh-catalysed hydroformylation using a static 10 mm reactor within a high-field magnet connected to liquid dosing and gas recirculation.[35]

Here, we investigate the hydroformylation of 1-hexene in the presence of $[Rh(acac)(CO)_2]$ and PPh_3 by *operando* high-resolution FlowNMR spectroscopy from an actively mixed pressure autoclave using periodic cycles of interleaved ^{1}H NMR, ^{31}P{^{1}H} NMR and selective excitation ^{1}H NMR measurements to gain insight into the speciation of the Rh/PPh_3 catalyst under reaction conditions.

Results and discussion

The hydroformylation of 1-hexene in the presence of $[Rh(acac)(CO)_2]$ and PPh_3 has been studied by FlowNMR spectroscopy under 12 bar of H_2/CO at 50 °C. The

experiments have been carried out as described in the ESI,† with [Rh(acac)(CO)$_2$] catalyst loadings of 2.5 mM and 1-hexene concentration of 500 mM corresponding to [S]/[Rh] = 200 (or 0.5 mol% cat.) throughout all experiments. The concentration of PPh$_3$ has been varied from 0–50 mM resulting in a ratio of [PPh$_3$]/[Rh] = 0–20. The autoclave was charged with 22.4 mL of non-deuterated toluene containing 100 mM of 1,3,5-trimethoxybenzene as internal standard. H$_2$ and CO were added separately in a 1 : 1 ratio.

The expected products from the reaction of 1-hexene with H$_2$/CO in the presence of [Rh(acac)(CO)$_2$] and PPh$_3$ resulting from hydrogenation, isomerization and hydroformylation are shown in Scheme 1. From previous investigations the predominance of hydroformylation can be expected under these conditions, along with some isomerization and possibly traces of hydrogenation.[36]

All reactions were carried out under batch conditions in a 100 mL thick-walled glass autoclave, with an aliquot of the reaction mixture continuously recirculating through the temperature-controlled FlowNMR tubing in a closed-loop (Fig. 3). This setup ensures the sample within the spectrometer is continually refreshed with access to the reagent gases in the headspace, making every solution fraction representative of the mixture in the reaction vessel with a *ca.* 30 s delay to the FlowNMR tube under typical reaction conditions (flow rate of 4 mL min^{-1}). Our modified setup enables working at temperatures of up to 140 °C and pressures of up to 20 bar (for details see the ESI†).

The first reaction was performed at 60 °C with 10 bar of H$_2$/CO (1 : 1), where the autoclave was initially pressurised with H$_2$ for 1 h before adding CO to trigger the hydroformylation reaction. After consideration of significant flow correction factors (see ESI†), reaction progress and chemoselectivity trends may be extracted from the NMR data (Fig. 4).

This initial experiment showed that high-resolution FlowNMR with an air-sensitive catalyst system is possible with a fully temperature-controlled and pressurized setup, allowed the identification of relevant NMR signals, and gave an indication of the reaction rate under the conditions applied. The identity of all of the organic products observed by ^{1}H NMR (*n*- and iso-heptanal, 2- and 3-hexene) were confirmed by GC-MS (see ESI†), which also ruled out formation of any significant quantities of other side products under the conditions used. Thus,
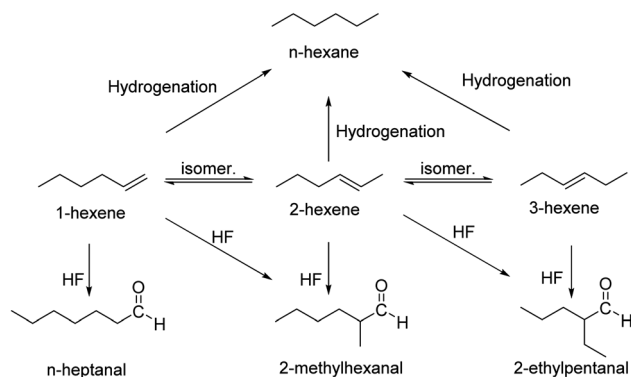
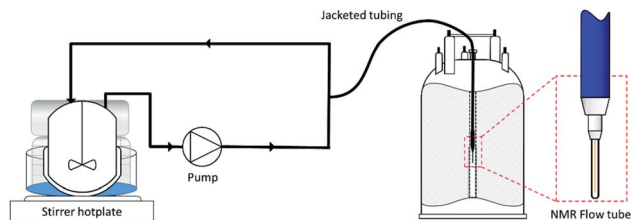Scheme 1 Possible primary reaction products from 1-hexene under hydroformylation conditions.

Fig. 3 Schematic of the FlowNMR apparatus (not to scale).

quantitative product distribution profiles may be plotted from the ^{1}H FlowNMR data (Fig. 5).

The observation of only isomerization of 1-hexene slowly occurring with k_{obs} = 0.90 mM min^{-1} immediately after adding H$_2$ suggests catalyst activation to a hydride complex to be fast, but without any appreciable hydrogenation activity (at 60 °C with 6 equiv. of PPh$_3$). Consumption of CO proceeded without any significant lag phase and hydroformylation smoothly progressed with a stable 3 : 1 linear/branched selectivity over the course of the reaction, alongside some continued isomerisation at k_{obs} = 0.36 mM min^{-1} until the end of the reaction. Maximum reaction rates were found in the first 40 min after the pressurisation with CO, with substrate consumption $k_{(obs)}^{1\text{-hexene}}$ = 8.76 mM min^{-1}, product formation $k_{(obs)}^{n\text{-heptanal}}$ = 6.43 mM min^{-1} and $k_{(obs)}^{2\text{-methylhexanal}}$ = 2.15 mM min^{-1}. These values as well as the observed aldehyde regioselectivity align well with previously reported data[16,36–40] and are consistent with previous kinetic studies.[22]

In the following studies the temperature was decreased to 50 °C and data acquisition optimised to increase temporal resolution. The reactor was
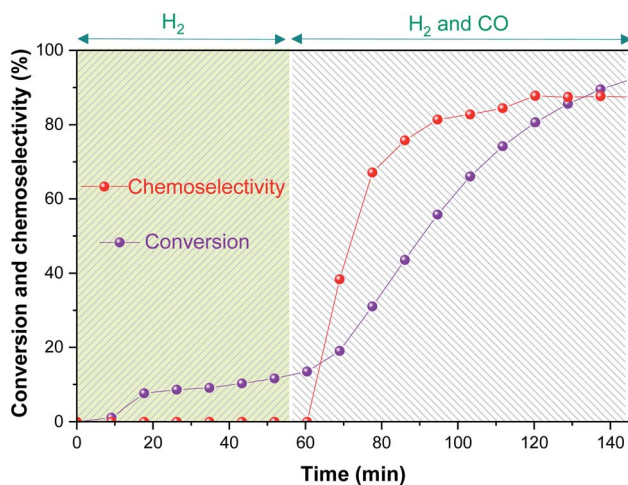

Fig. 4 Substrate conversion and chemoselectivity to aldehydes of the [Rh(CO)$_2$(acac)] + 6PPh$_3$ catalysed hydroformylation of 1-hexene in toluene at 60 °C and 10 bar of H$_2$/CO (1 : 1) monitored using *operando* ^{1}H FlowNMR spectroscopy. [Rh(CO)$_2$(acac)] = 2.5 mM, [PPh$_3$] = 15 mM, [1-hexene] = 500 mM. From t = 5–55 min only 5 bar H$_2$ were present, after which another 5 bar CO were added.
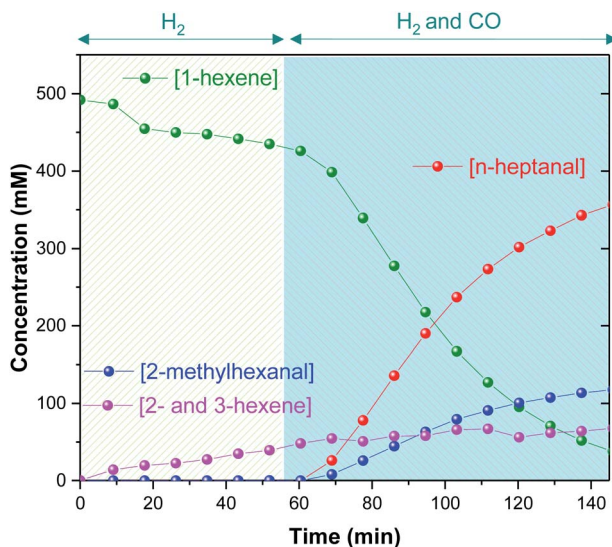
Fig. 5 Product formation and substrate consumption profiles of [Rh(CO)$_2$(acac)] + 6PPh$_3$ catalysed hydroformylation of 1-hexene in toluene at 60 °C and 10 bar of H$_2$/CO (1 : 1) monitored using *operando* ^{1}H FlowNMR spectroscopy. [Rh(CO)$_2$(acac)] = 2.5 mM, [PPh$_3$] = 15 mM, [1-hexene] = 500 mM.

pressurized with both gases (12 bar 1 : 1 H$_2$/CO) at the same time to immediately start the hydroformylation. A series of experiments were conducted where the amount of PPh$_3$ was varied under otherwise identical conditions (Fig. 6).
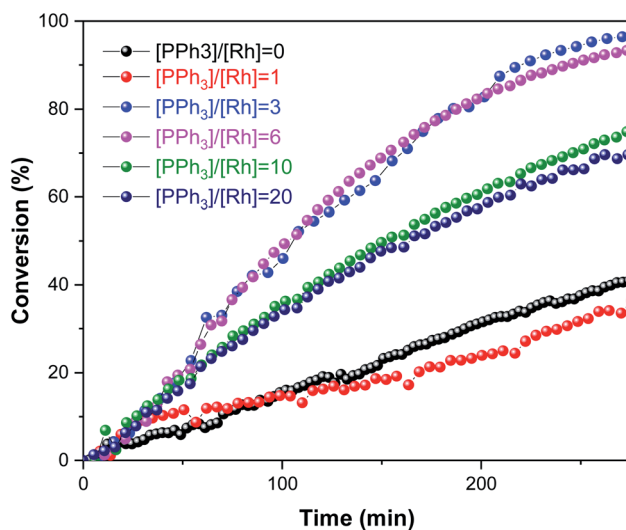

Fig. 6 Substrate conversion profiles of [Rh(CO)$_2$(acac)] + PPh$_3$ catalysed hydroformylation of 1-hexene in toluene at 50 °C and 12 bar of H$_2$/CO (1 : 1) monitored using *operando* ^{1}H FlowNMR spectroscopy. [Rh(CO)$_2$(acac)] = 2.5 mM, [1-hexene] = 500 mM, [PPh$_3$] varied as indicated.

As expected, the amount of PPh$_3$ added had a non-linear influence on the activity. With no phosphine present the Rh catalyst yielded some aldehyde production with a moderate L/B ratio of 2.4 : 1 in the first 30 min of the reaction, but mostly produced 3-hexene that did not undergo hydroformylation (Fig. 7); this behaviour is known for [RhH(CO)$_4$] catalysed hydroformylation.[39] With one equivalent of PPh$_3$ added the system afforded a similar rate (Fig. 6), but with much higher chemoselectivity for aldehyde production with increased L/B ratios (Fig. 7). Under these conditions some isomerisation still occurred alongside hydroformylation, leading to decreasing L/B ratios over time as the 2-hexene formed underwent hydroformylation to 2-methylhexanal (Fig. 7). With 3–6
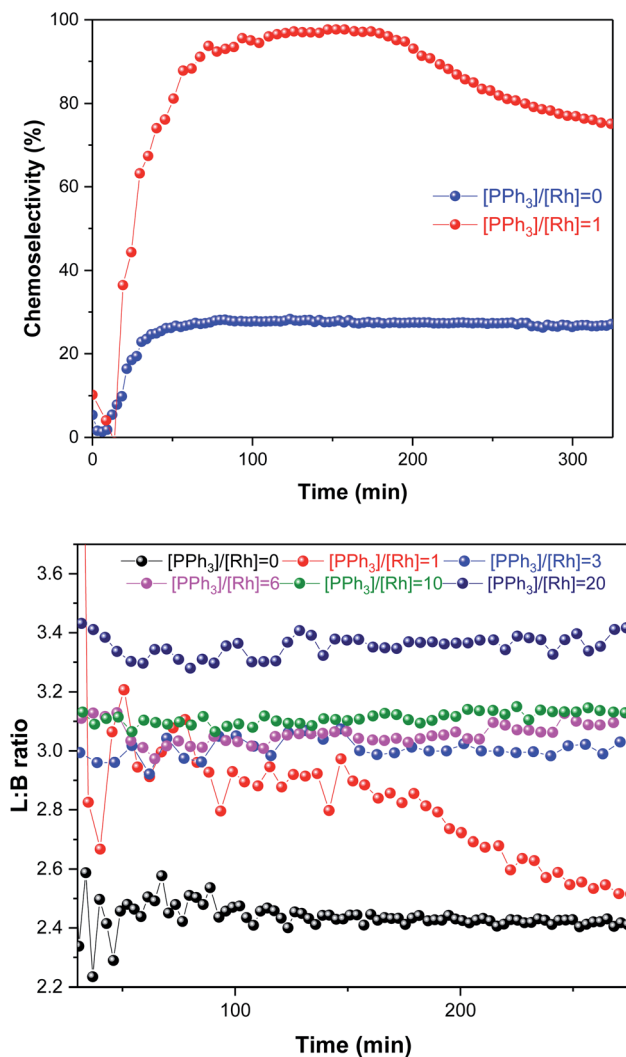

Fig. 7 Aldehyde chemoselectivity (upper) and regioselectivity profiles (lower) of [Rh(CO)$_2$(acac)] + PPh$_3$ catalysed hydroformylation of 1-hexene in toluene at 50 °C and 12 bar of H$_2$/CO (1 : 1) monitored using *operando* ^{1}H FlowNMR spectroscopy. [Rh(CO)$_2$(acac)] = 2.5 mM, [1-hexene] = 500 mM, [PPh$_3$] varied as indicated.

equivalents of PPh_3/Rh the rate of 1-hexene consumption was about four times higher, with >95% chemoselectivity to aldehyde formation at stable L/B ratios of 3 : 1 at 50 °C. When 10–20 equivalents of PPh_3 were added high chemo- and regio-selectivities were maintained, but at reduced overall reaction rates due to PPh_3 competing with the olefin substrates for coordination to the Rh centre. Again, this behaviour is well documented in the literature,[41] and the overall rates observed in our FlowNMR studies (Table S4†) are in line with previous reports.[37]

As in some of our previous work,[42] it was also possible to track the amount of H_2 dissolved in solution by ^1H FlowNMR during the hydroformylation reaction (Fig. 8) after considering flow effects and the ortho/para ratio of H_2 at 50 °C.[43] Ensuring that the volume element analysed in the NMR (temporarily disconnected from the autoclave headspace) is still under turnover conditions and not deprived of any reagent is important to ascertain that the results obtained are truly *operando* and not just *in situ*. From the concentration plots shown in Fig. 9 it can be seen that dissolution of H_2 into solution was rapid under the conditions applied, and because the reactor had been sealed after the initial pressurisation, its decreasing concentration over time tracked the amount of H_2 consumption by the reaction. Although we have not quantified the gas–liquid distribution of the system, the lower H_2 uptake by the reaction without PPh_3 concurs with the observation of mainly olefin isomerisation occurring. Even for the faster reactions with 3–6 equivalents of PPh_3 that did consume H_2/CO in producing aldehydes, the system never entered a gas-limited regime showing effective mixing.

Under the conditions applied, the reaction is believed to proceed *via* a dissociative mechanism (Scheme 2)[27,44,45] initially proposed by Wilkinson for ethylene as the substrate,[22] analogous to Heck's mechanism for Co-catalysed hydroformylation.[46]
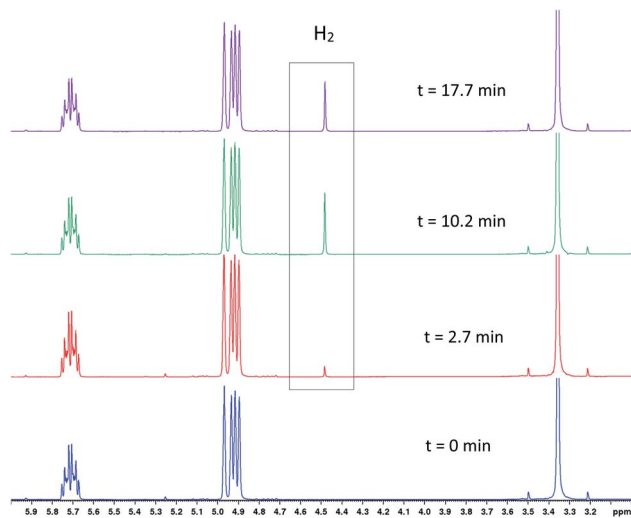

Fig. 8 ^1H NMR spectra showing the appearance of dissolved H_2 during [Rh(CO)$_2$(acac)] + 6PPh$_3$ catalysed hydroformylation of 1-hexene in toluene at 50 °C and 12 bar of H_2/CO (1 : 1) from *operando* ^1H FlowNMR spectroscopy. [Rh(CO)$_2$(acac)] = 2.5 mM, [PPh$_3$] = 15 mM, [1-hexene] = 500 mM.
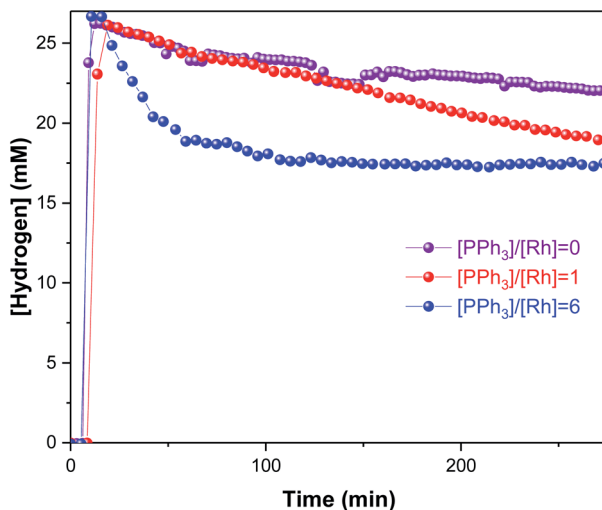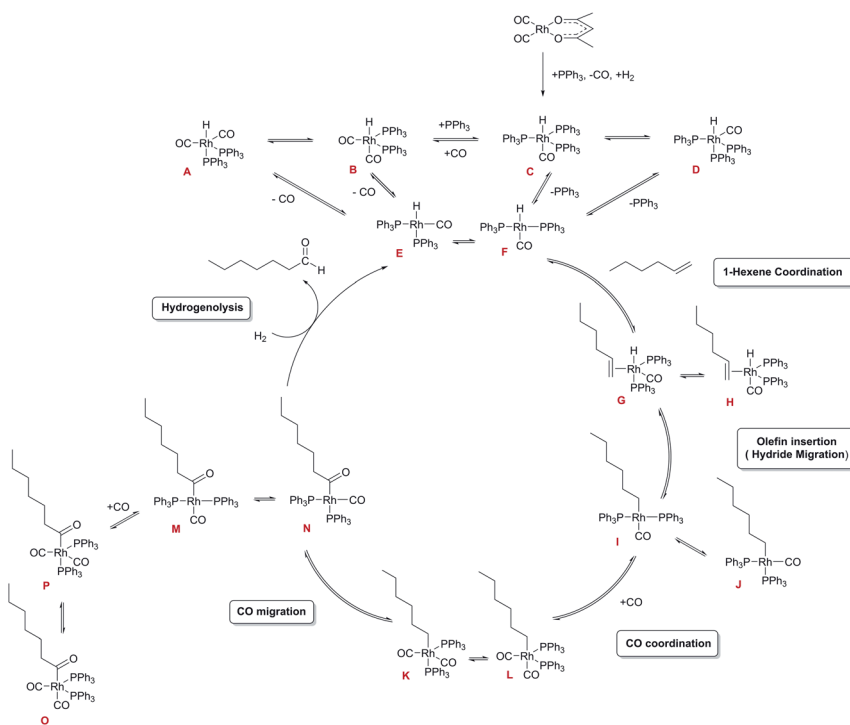
Fig. 9 Hydrogen concentration profiles during [Rh(CO)$_2$(acac)] + PPh$_3$ catalysed hydro-formylation of 1-hexene in toluene at 50 °C and 12 bar of H$_2$/CO (1 : 1) monitored using *operando* ^{1}H FlowNMR spectroscopy. [Rh(CO)$_2$(acac)] = 2.5 mM, [1-hexene] = 500 mM, [PPh$_3$] varied as indicated.

Scheme 2 Simplified dissociative mechanism for the Rh-catalysed hydroformylation of hexene (only heptanal formation shown). All in-cycle reaction intermediates are believed to contain two PPh$_3$ ligands per Rh.

The mechanism starts with the formation of unsaturated complexes **E** and **F** by dissociation of CO or ligand from stable five-coordinate Rh^{I} hydrido-carbonyl complexes. Thereafter, the olefin coordinates to give the olefin-hydrido-carbonyl complexes **G** and **H** that can undergo intramolecular hydride migration to form the alkyl complexes **I** and **J**. Coordination of CO to **I** and **J** results in the alkyl-carbonyl complexes **K** and **L** that can undergo a migratory CO insertion to form acyl complexes **M** and **N** which may coordinate additional CO to form the more stable five-coordinate acyl complexes **O** or **P**. The last step to complete the cycle is the hydrogenolysis to release the aldehyde and recover complexes **E** and **F**. The latter is generally believed to be the only irreversible process and constitutes the turnover limiting step in the cycle.[22] Among the various intermediates proposed throughout the catalytic cycle, only the penta-coordinated complex $[RhH(CO)(PPh_3)_3]$ **C** has been fully characterized by NMR and IR spectroscopy as well as X-ray crystallography.[44,47,48] The related $[RhH(CO)_2(PPh_3)_2]$ complexes **A** and **B** have been characterized by NMR and IR spectroscopy in solution due to their fluxional behaviour caused by the rapid exchange of PPh_3 ligands from equatorial to axial positions.[49,50] The in-cycle acyl rhodium complex $[Rh\{CO(CH_2)_5(CH_3)\}(CO)_2(PPh_3)_2]$ **P** has been identified by NMR spectroscopy, in addition to some off-cycle dinuclear Rh species such as $[Rh_2(CO)_4(PPh_3)_4]$, $[Rh_2(CO)_5(PPh_3)_3]$ and $[Rh_2(CO)_6(PPh_3)_2]$.[27,51] For the PCy_3 ligand the tetra-coordinated complex $[RhH(CO)(PCy_3)_2]$ has been synthesised and monitored spectroscopically under hydroformylation conditions,[52] although this catalyst is very slow due to the bulky, strongly binding trialkylphosphine.

In order to gain some insight into the speciation of the $[Rh(acac)(CO)_2]/PPh_3$ catalyst system during catalysis we measured selectively excited ^1H NMR spectra[53] focussing on the negative shift region where Rh–H resonances are expected, and also acquired $^{31}P\{^1H\}$ NMR spectra during the reaction in flow. With optimised acquisition parameters using a 500 MHz spectrometer fitted with a cryoprobe (see ESI for details†) we were able to acquire these alongside the standard ^1H FlowNMR for monitoring reaction progress in a sequential manner throughout the reaction in a single experiment at 2.5 mM [Rh] concentration in non-deuterated solvent. The hydride FlowNMR spectra thus acquired at 50 °C showed the smooth growth of a broad singlet peak centred at −9.18 ppm (12 Hz FWHM) over the course of the reaction (Fig. 10).
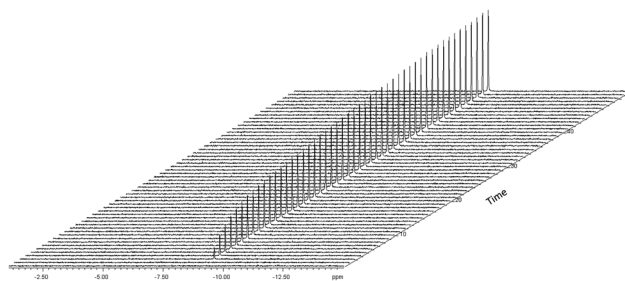

Fig. 10 Rhodium–hydride formation during $[Rh(CO)_2(acac)] + 6PPh_3$ catalysed hydroformylation of 1-hexene in toluene at 50 °C and 12 bar of H_2/CO (1 : 1) monitored using selective excitation ^1H FlowNMR spectroscopy. $[Rh(CO)_2(acac)] = 2.5$ mM, $[1\text{-hexene}] = 500$ mM, $[PPh_3] = 15$ mM.

This hydride signal appeared immediately after adding syngas to the reaction mixture, but not with H_2 alone. No other hydride resonances were detected, and the same signal was observed for any P/Rh ratios >1. For 1 and 0 equivalents of PPh_3, no hydride signals were detected. The absence of any defined Rh–H coupling patterns in the broad singlet at −9.18 ppm is expected due to the known low magnitude of $^1J_{RhH}$ of <10 Hz.[54]

The corresponding $^{31}P\{^1H\}$ FlowNMR spectra of mixtures of $[Rh(acac)(CO)_2]$ and PPh_3 did not show any signals in the absence of syngas, likely due to rapid chemical exchange between a number of unknown species (bubbling indicative of CO release can be observed visually upon combining $[Rh(acac)(CO)_2]$ and PPh_3). Immediately after pressurising the mixture with syngas the $^{31}P\{^1H\}$ FlowNMR spectra regained shape and showed three major resonances: a large, broad singlet peak at −4.9 ppm (68.5 Hz FWHM) originating from free PPh_3, a small sharp singlet at 25.1 ppm from traces of PPh_3 oxide (as verified with an authentic sample), and a well-defined doublet with a coupling constant of 139.2 Hz centred at 37.3 ppm (Fig. 11).

The growth of the $^{31}P\{^1H\}$ doublet at 37.3 ppm tracked the appearance of the broad ^1H signal at −9.18 ppm. ^{31}P DOSY and ^1H DOSY spectra showed very similar diffusion coefficients of 7.7×10^{-10} m^2 s^{-1} and 7.1×10^{-10} m^2 s^{-1} for both (see Fig. S15 and S16†), but the apparent absence of any $^2J_{PH}$ coupling in the ^1H signal initially seemed surprising. A ^1H–^{31}P HMBC spectrum did however clearly establish both resonances to originate from the interchanging coordination isomers **A** ↔ **B** of $[RhH(CO)_2(PPh_3)_2]$ (Fig. 12). The rapid intramolecular exchange of the PPh_3 between equatorial and apical positions, known to be facile in trigonal-bipyramidal Rh(I) complexes by way of Berry pseudo-rotation, obscures the observation of any $^2J_{PH}$ couplings in this complex under syngas at 50 °C.[49,50] Additional intermolecular exchange with free PPh_3 (**A** ↔ **B** ↔ **C** ↔ **D** as indicated by the slightly broadened $^{31}P\{^1H\}$ signal at −4.9 ppm) may contribute further to the fluxionality of this complex.
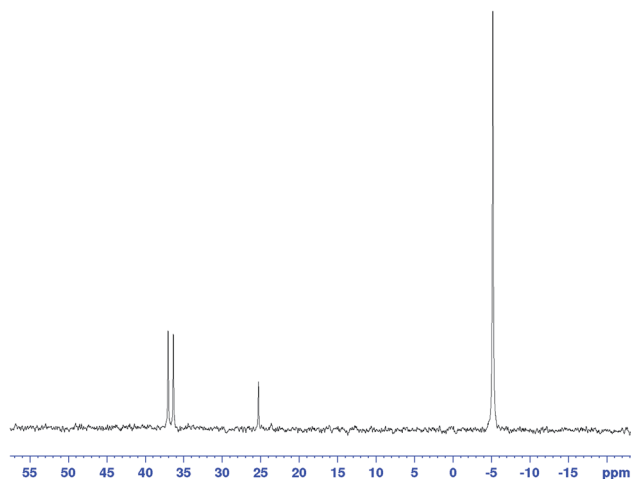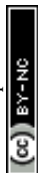

Fig. 11 $^{31}P\{^1H\}$ FlowNMR spectrum recorded during $[Rh(CO)_2(acac)]$ + 6PPh$_3$ catalysed hydroformylation of 1-hexene in toluene at 50 °C and 12 bar of H_2/CO (1 : 1) at $t = $ 395 min. $[Rh(CO)_2(acac)]$ = 2.5 mM, [1-hexene] = 500 mM, [PPh$_3$] = 15 mM.

Fig. 12 $^1H-^{31}P$ HMBC NMR spectrum recorded during [Rh(CO)$_2$(acac)] + 6PPh$_3$ catalysed hydroformylation of 1-hexene in toluene at 50 °C and 12 bar of H$_2$/CO (1 : 1) at t = 325 min. [Rh(CO)$_2$(acac)] = 2.5 mM, [1-hexene] = 500 mM, [PPh$_3$] = 15 mM.
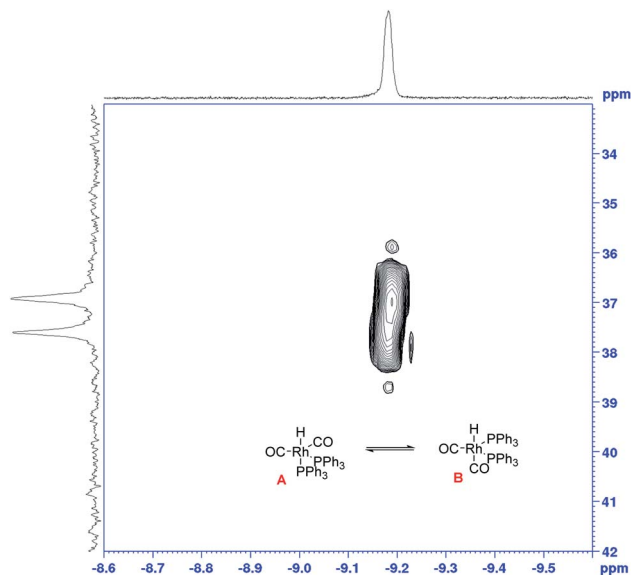
To test the connectivity of **A/B** to the catalytic cycle, one flow run was deliberately interrupted by stopping the pump to temporarily isolate the sample in the magnet from the gas supply in the reactor headspace. From the ^1H FlowNMR spectra it could be seen that the reaction progressed for about 2 min until the H$_2$ (and presumably CO) dissolved in solution had been consumed (Fig. 13). Once the sample in the tip of the flow tube had run out of syngas, both the ^{31}P and ^1H signals of the hydrido-carbonyl complexes **A/B** started to fade away from the spectra (Fig. 13). As soon as flow was resumed and the sample fed back into the reactor where it was brought into contact with syngas again, hydroformylation activity resumed accompanied by re-appearance of [RhH(CO)$_2$(PPh$_3$)$_2$]. This experiment demonstrated this complex to be of direct relevance to the catalytic cycle, representing the major reaction intermediate under the conditions applied.

When the excess H$_2$/CO was vented at the end of the reaction (after complete consumption of hexene) and the sample analysed under an atmosphere of argon, the only Rh–phosphine species detected by NMR was the known [RhH(CO)(PPh$_3$)$_3$] complex **C** resulting from substitution of one CO by PPh$_3$. However, when the catalyst was deprived of syngas mid-reaction (*i.e.* in the presence of hexene substrate) as described above, no hydride resonance could be observed at all in the selectively excited ^1H NMR, but a new signal was detected in the $^{31}P\{^1H\}$ NMR. Interestingly, it was the same species that was the only Rh–phosphine complex detected by FlowNMR throughout the reaction when PPh$_3$/Rh = 1 (Fig. 14). The doublet peak centred at 27.7 ppm had a relatively low $^1J_{RhP}$ of 71.8 Hz and no associated hydride signal.

The conditions under which this complex was observed together with its spectroscopic signatures suggested that it may be an acyl intermediate prior to
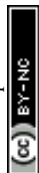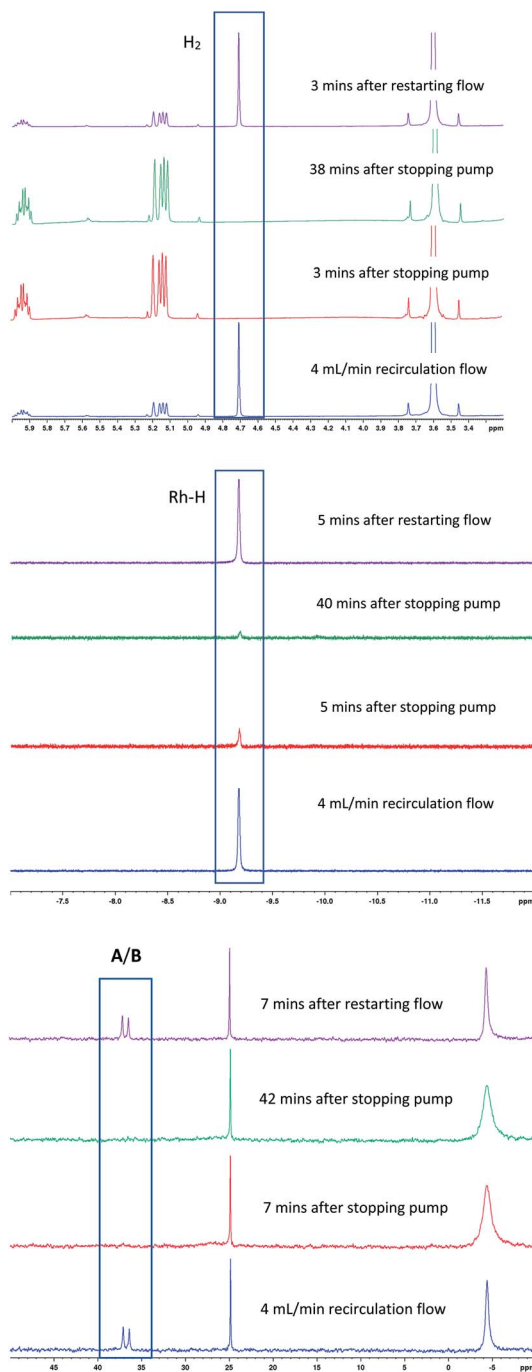
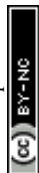**Fig. 13** ^{1}H and ^{31}P{^{1}H} FlowNMR spectra of [Rh(CO)$_2$(acac)] + 6PPh$_3$ catalysed hydro-formylation of 1-hexene in toluene at 50 °C and 12 bar of H$_2$/CO (1 : 1) during stop/start cycling of flow. [Rh(CO)$_2$(acac)] = 2.5 mM, [1-hexene] = 500 mM, [PPh$_3$] = 15 mM.
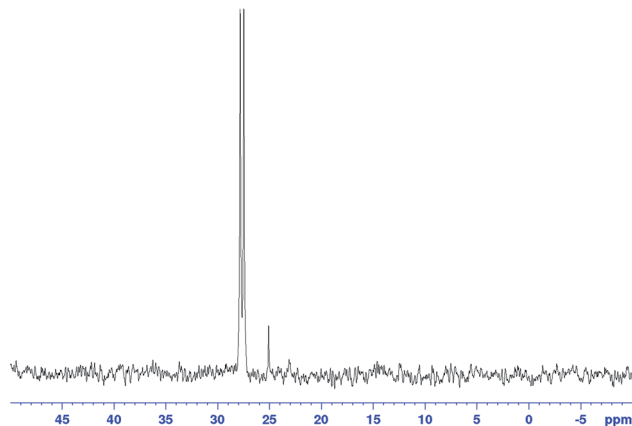
Fig. 14 ^{31}P{^{1}H} FlowNMR spectrum recorded during [Rh(CO)$_2$(acac)] + 1PPh$_3$ catalysed hydroformylation of 1-hexene in toluene at 50 °C and 12 bar of H$_2$/CO (1 : 1). The same doublet at 27.7 ppm was also observed from mixtures with higher PPh$_3$/Rh ratios when deprived of syngas in the presence of 1-hexene. [Rh(CO)$_2$(acac)] = 2.5 mM, [1-hexene] = 500 mM, [PPh$_3$] = 2.5 mM.

release of product *via* hydrogenolysis (**O–N**, Scheme 2). Indeed, a very similar ^{31}P {^{1}H} NMR signal (doublet at 27.5 ppm with $^1J_{RhP}$ = 78.0 Hz) had previously been assigned to [Rh(CO(CH$_2$)$_5$CH$_3$)(CO)$_2$(PPh$_3$)$_2$] but not fully characterised.[27] A ^{31}P DOSY spectrum gave a diffusion coefficient of 7.35 × 10^{-10} m^2 s^{-1} for our signal at 27.7 ppm (Fig. S17†), very similar to the monomeric [RhH(CO)$_2$(PPh$_3$)$_2$] complexes **A/B** analysed under the same conditions.

When the stable complex [RhH(CO)(PPh$_3$)$_3$] **C** was pressurised with CO in the presence of 1-hexene but without H$_2$ under otherwise identical reaction conditions, **C** disappeared from the ^{1}H spectra with a transient trace of **A/B** before all hydride signals vanished (Fig. 15). The corresponding ^{31}P{^{1}H} NMR spectra showed the same sequence of transformation, eventually yielding the doublet at 27.7 ppm along with one equivalent of OPPh$_3$ at 24 ppm and one equivalent of PPh$_3$ at −4.9 ppm (Fig. 15). From this observation we can deduce that only one PPh$_3$ is coordinated to the Rh centre in this compound thus identified as the acyl complex [Rh(CO(CH$_2$)$_5$CH$_3$)(CO)$_3$(PPh$_3$)] (**Q**). As expected, no aldehyde formation was observed in this experiment. Pressurising the mixture with CO and H$_2$ immediately led to hydroformylation activity with the acyl complex **Q** disappearing and **A/B** dominating the phosphorus and hydride FlowNMR spectra just as when starting from [Rh(acac)(CO)$_2$] + PPh$_3$ (see Fig. 10 and 11).

The observation of a mono-phosphine acyl complex as the major catalyst species prior to rate-limiting hydrogenolysis is surprising given the long-accepted view that all in-cycle intermediates in Wilkinson's dissociative mechanism would be bis-phosphine complexes (Scheme 2).[27,45] In support of this notion, Brown reported the NMR spectroscopic characterisation of bis-phosphine acyl complex **P** obtained from [RhHCO(PPh$_3$)$_3$] (**C**) and 1-octene under atmospheric pressure of ^{13}CO.[44] However, the facile displacement of PPh$_3$ by CO observed in the generation of **A/B** from **C** under 5 bar of CO (Fig. 15) suggests that a similar equilibrium may generate mono-phosphine complexes from Brown's bis-phosphine complex under catalytic reaction conditions of >1 bar CO.
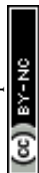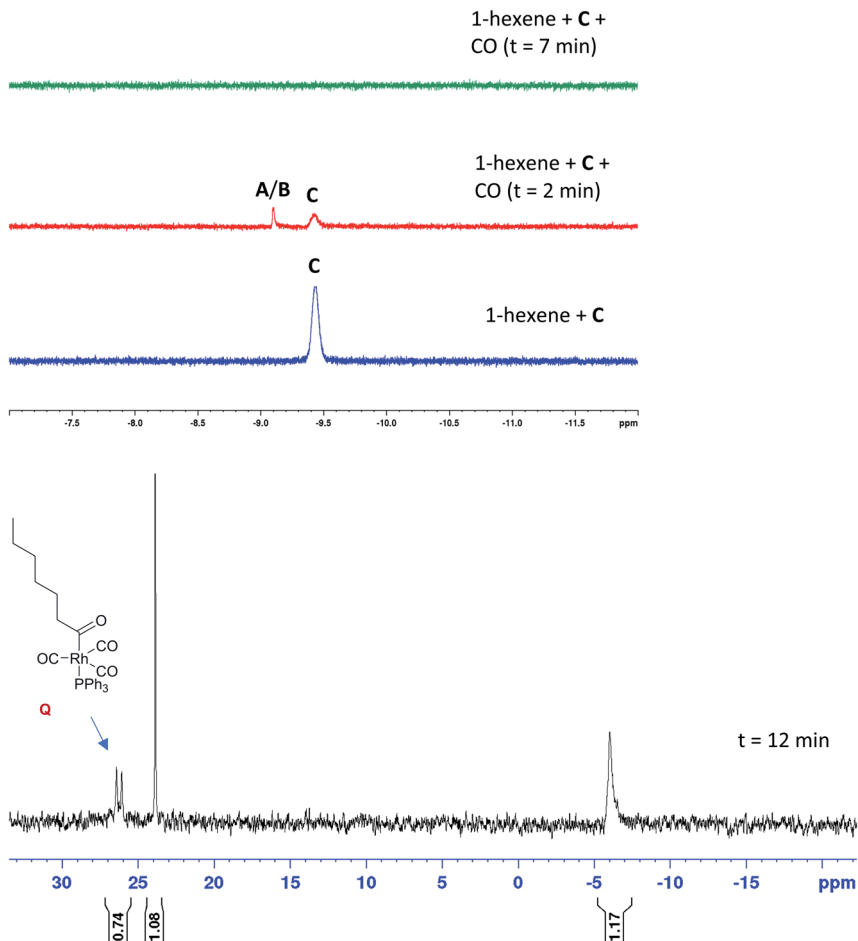
Fig. 15 Selective excitation ^{1}H and ^{31}P{^{1}H} FlowNMR spectra of [RhH(CO)(PPh$_3$)$_3$] (2.5 mM) and 1-hexene (500 mM) under 6 bar of CO in toluene at 50 °C.

In order to confirm this hypothesis and ascertain the structural identity of **Q** as a mono-phosphine acyl complex we reacted [RhHCO(PPh$_3$)$_3$] (**C**) and 1-hexene with 5 bar of 99.9% enriched ^{13}C carbon monoxide in toluene. As seen before (Fig. 15), the hydride signal of **C** vanished within minutes after pressurising **C** with ^{13}CO in the presence of olefin, transiently showing the formation of **A/B** (Fig. 16) before all hydride signals disappeared after 60 min at 25 °C. With two ^{13}CO ligands the ^{1}H resonance of **A/B** was a triplet of doublets with a $^2J_{CH} = 30.2$ Hz and $^1J_{RhH} = 3.9$ Hz without any apparent $^2J_{PH}$ due to the fluxionality of this complex (as discussed above).

The corresponding ^{31}P{^{1}H} NMR spectra showed the same sequence of transformations, eventually yielding a virtual triplet of quartets centred at 26.5 ppm along with some OPPh$_3$ at 25 ppm and free PPh$_3$ at −4 ppm (Fig. 17) as seen before for **Q** (Fig. 15). The ^{31}P resonance associated with the acyl complex coincidentally showed identical $^1J_{RhP} = 70.7$ Hz and $^2J_{PC} = 70.7$ Hz couplings to the *trans* acyl carbon, and a distinct *cis* $^2J_{PC} = 17.6$ Hz from coupling to three

A/B

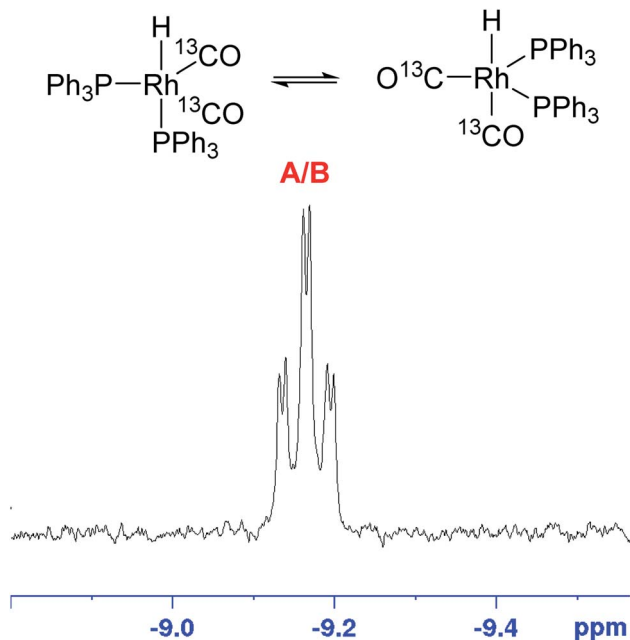Fig. 16 Selective excitation ^{1}H NMR spectrum of [RhH(CO)(PPh$_3$)$_3$] (25 mM) and 1-hexene (500 mM) under 5 bar of ^{13}CO in 0.5 mL of toluene at 0 °C showing the transient formation of **A/B** from **C** with ^{13}CO.

equivalent ^{13}CO ligands. This multiplicity is only possible with a pentacoordinate mono-phosphine tris-carbonyl acyl complex as drawn for **Q**.

The corresponding ^{13}C{^{1}H} NMR spectra showed a variety of distinct carbonyl species in the range of 240–180 ppm (Fig. 18). Free ^{13}CO dissolved in toluene was

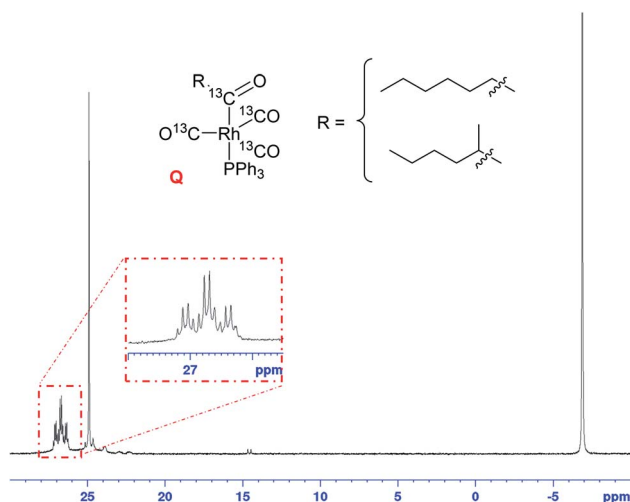Fig. 17 ^{31}P{^{1}H} NMR spectrum of [RhH(CO)(PPh$_3$)$_3$] (25 mM) and 1-hexene (500 mM) under 5 bar of ^{13}CO in toluene at −40 °C, showing the formation of **Q** from **C** with ^{13}CO.

observed at 184.5 ppm (confirming excess conditions), and the quaternary carbonyls of heptanal and 2-methylhexanal originating from stoichiometric 1-hexene hydroformylation were observed at 200.5 ppm and 203.2 ppm in a 3 : 1 ratio, respectively. The terminal ^{13}CO ligands of mono-phosphine complex **Q** were observed as two overlapping doublets of doublets at 192.1 ppm with $^{1}J_{RhC} = 74.5$ Hz and $^{2}J_{CP} = 17.5$ Hz as well as $^{1}J_{RhC} = 74.7$ Hz and $^{2}J_{CP} = 17.3$ Hz, confirming the *cis* $^{2}J_{PC}$ observed in the $^{31}P\{^{1}H\}$ NMR spectra (Fig. 17). Interestingly, while only one version of **Q** was detectable in the $^{31}P\{^{1}H\}$ NMR spectra, the two different acyl regio-isomers **Q_L** and **Q_B** could just be distinguished in the $^{13}C\{^{1}H\}$ NMR spectra in the expected 3 : 1 ratio (with similar chemical shifts and *cis* $^{2}J_{PC}$ couplings), consistent with the formation of linear and branched aldehydes.

Although not visible in the corresponding $^{31}P\{^{1}H\}$ NMR spectra due to very fast exchange between axial and equatorial positions, the $^{13}C\{^{1}H\}$ doublet at 198.36 ppm with a $^{1}J_{RhC} = 76.7$ Hz could be assigned to the terminal ^{13}CO ligands of the bis-phosphine complex **O/P** previously reported by Brown.[44] Upon cooling the sample to -90 °C, coupling of ^{13}CO with ^{31}P could be resolved as a doublet of triplets with a *cis* $^{2}J_{CP} = 20.9$ Hz (Fig. S29†) but the corresponding $^{31}P\{^{1}H\}$ signal of **O/P** could still not be detected. The ratio of **Q** to **O/P** in the $^{13}C\{^{1}H\}$ NMR spectra was about 1.3 : 1 under 5 bar of ^{13}CO in the presence of 3 equiv. of PPh$_3$ per Rh, similar to the formation of **A/B** from **C** in the presence of excess CO (Fig. 15). Consistent with our assignments, the ^{13}C resonances of the terminal acyls in both regio-isomers of **Q** and **O/P** could be detected in in the range of 225–240 ppm (Fig. 18), showing characteristic C–Rh and C–P coupling constants despite partial signal overlap (Fig. S30†). Similar to the difficulty of resolving P–H couplings in
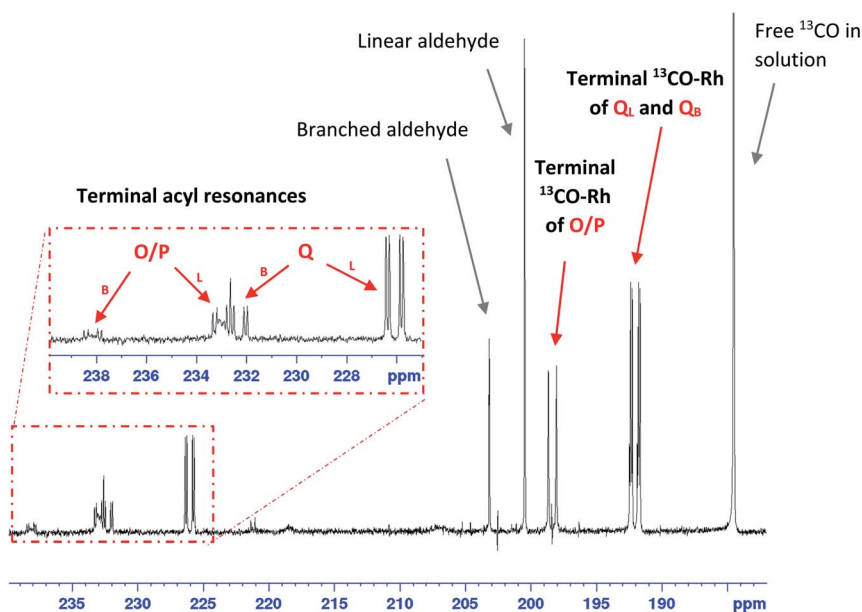

Fig. 18 $^{13}C\{^{1}H\}$ NMR spectrum of [RhH(CO)(PPh$_3$)$_3$] (25 mM) and 1-hexene (500 mM) under 5 bar of ^{13}CO in toluene at -40 °C showing the formation of **Q** and **O/P** from **C** with ^{13}CO.

Paper

the rapidly interconverting isomers of **A/B** (Fig. 11), no C–C couplings between the acyl and terminal carbonyls could be resolved in the ^{13}C{^{1}H} NMR spectra of **Q** and **O/P** down to −40 °C due to their highly fluxional nature (all ^{13}C{^{1}H} NMR signals including free ^{13}CO were very broad at room temperature; Fig. S31†). Further confirmation of the assignment of **Q** as a mixture of two regio-isomers of a mono-phosphine acyl complex and **O/P** as a mixture of isomers of bis-phosphine acyl complexes came from ^{1}H–^{13}C HMBC and ^{1}H–^{31}P HMBC correlation experiments (Fig. S32 and S33†) as well as a quantitative ^{13}C{^{1}H} 1D NMR measurement showing a 2 : 1 CO/acyl ratio for **O/P** and 3 : 1 CO/acyl ratio for **Q** in their relative peak integrals (Fig. S35†).

The dynamic equilibrium between **Q** and **O/P** was shown by a change in their distribution from 1.3 : 1 under 5 bar CO to 1 : 2.5 after the excess CO was vented from the mixture (Fig. S34†). The different conditions used in Brown's experiments[44] and our own thus explain the different complexes detected. At higher PPh$_3$ loadings of >3 equiv. to Rh (as typically used in applied hydroformylation) the excess phosphine might overcompensate for the higher CO pressures and shift the equilibrium to the bis-phosphine acyl complex again. When a total of 6 equivalents of PPh$_3$ to Rh were used under 5 bar of ^{13}CO, the ratio of **Q** to **O/P** in the ^{13}C{^{1}H} NMR spectra was found to be 1 : 3 as opposed to 1.3 : 1 with 3 equiv. PPh$_3$, clearly showing the coordination competition of CO and PPh$_3$ in **Q** vs. **O/P** just as in **C** vs. **A/B** (Scheme 3).

These observations provide evidence for several conclusions: (i) olefin coordination does not occur with the off-cycle tris-PPh$_3$ complex **C** but requires
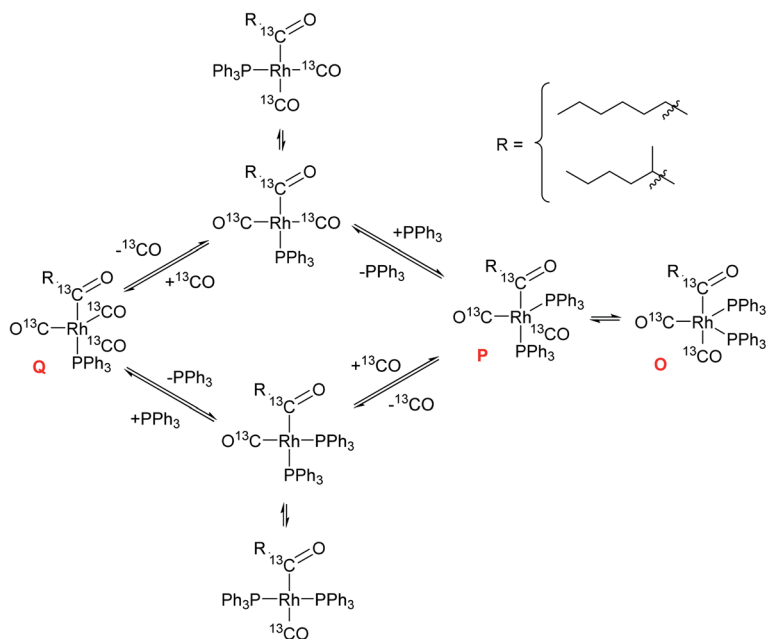
Scheme 3 Coordination equilibria between the mono- (**Q**) and bis-phosphine (**O/P**) acyl complexes through dynamic PPh$_3$ and CO exchange (unlabelled four-coordinate intermediates not detected but believed to be the species reacting further with H$_2$, see Scheme 2).
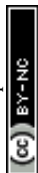
dissociation of at least one PPh_3, a process that is facilitated by excess CO; (ii) once bis-phosphine hydrido–carbonyl complexes **A/B** have been generated they lead into the catalytic cycle, where the sequence of olefin coordination – hydride migration – CO insertion proceeds rapidly through either bis- or mono-phosphine intermediates; (iii) both mono- and bis-phosphine acyl complexes **Q** and **O/P** are observable as in-cycle intermediates prior to rate-limiting hydrogenolysis, with their ratios depending on the relative amounts of CO and PPh_3 present; (iv) the observation that hydroformylation rates are highest under conditions that see **Q** dominating over **O/P** (PPh_3/Rh = 3 at 5 bar CO) at unchanged L/B selectivity suggests that hydrogenolysis proceeds predominantly through mono-phosphine acyl intermediates.

Conclusion

The results of this investigation of one of the most widely used homogeneous catalytic systems extend multi-nuclear high-resolution FlowNMR spectroscopy to high temperature systems operating under gas pressure. While not as sensitive as gas chromatography and mass spectrometry or as fast as IR spectroscopy, FlowNMR is inherently quantitative, non-invasive and highly informative and thus powerful for following similar reaction intermediates with high specificity. Being able to quantify dissolved H_2 during the analysis is uniquely useful in ensuring true *operando* conditions, and may be exploited to map out gas-limitation regimes to guide process development and upscaling. The ability to temporarily isolate a sample from the headspace by interruption of flow allows probing the behaviour of the system under gas-limiting conditions and following associated changes in catalyst speciation. Heteronuclear correlation experiments and diffusion measurements may be used to characterise fleeting reaction intermediates and gain insights into their dynamics. In the case of Rh/PPh_3 catalysed hydroformylation of 1-hexene, this approach has led to the successful characterisation of $[RhH(CO)(PPh_3)_3]$, $[RhH(CO)_2(PPh_3)_2]$ as well as bis- and mono-phosphine acyl intermediates under reaction conditions for the first time. Work to further extend the utility of high-resolution FlowNMR spectroscopy to study hydroformylation and other catalytic systems is currently ongoing in our laboratories.
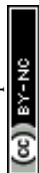
Conflicts of interest

RF is an employee of Evonik GmbH who operate industrial hydroformylation plants. The other authors declare no conflicts of interest.

Note after first publication

The data in Fig. 16–18 and Scheme 3, and the related discussion, was presented at the Faraday Discussions meeting and added to the manuscript post-meeting.

Acknowledgements

References

1 H. Adkins and G. Krsek, *J. Am. Chem. Soc.*, 1949, **71**, 3051–3055.

2 R. Franke, D. Selent and A. Börner, *Chem. Rev.*, 2012, **112**, 5675–5732.

3 O. Roelen, Chemische Verwertungsgesellschaft Oberhausen m.b.H., DE 849548, 1938 & 1952; *US Pat.* 2327066, 1943; *Chem. Abstr.*, 1944, **38**, 3631.

4 L. Stahl, *J. Am. Chem. Soc.*, 2007, **129**, 10297–10298.

5 P. C. J. Kamer, J. N. H. Reek and P. W. N. M. van Leeuwen, *Rhodium Catalyzed Hydroformylation*, Springer International Publishing, 2005.

6 G. R. Stephenson, *Organometallic chemistry: The transition elements*, 1996.

7 G. Morales Torres, R. Frauenlob, R. Franke and A. Börner, *Catal. Sci. Technol.*, 2015, **5**, 34–54.

8 G. Süss-Fink, in *Homogeneous Transition Metal Catalyzed Reactions*, American Chemical Society, 1992, vol. 230, pp. 28–419.

9 M. Beller, B. Cornils, C. D. Frohning and C. W. Kohlpaintner, *J. Mol. Catal. A: Chem.*, 1995, **104**, 17–85.

10 S. Naqvi, *Oxo Alcohols. Process Economics Program Report 21E*, 2010.

11 H. K. Reinius, P. Suomalainen, H. Riihimäki, E. Karvinen, J. Pursiainen and A. O. I. Krause, *J. Catal.*, 2001, **199**, 302–308.

12 A. Nemati Kharat, F. Rajabi Kouchi and B. Tamaddoni Jahromi, *J. Coord. Chem.*, 2016, **69**, 12–19.

13 P.-A. R. Breuil, L. Magna and H. Olivier-Bourbigou, *Catal. Lett.*, 2015, **145**, 173–192.

14 I. Ojima, *Chem. Rev.*, 1988, **88**, 1011–1030.

15 M. Diéguez, O. Pàmies and C. Claver, *Tetrahedron: Asymmetry*, 2004, **15**, 2113–2122.

16 A. A. Dabbawala, R. V. Jasra and H. C. Bajaj, *Catal. Commun.*, 2011, **12**, 403–407.

17 R. Whyman, *Appl. Organomet. Chem.*, 2001, **15**, 315–316.

18 L. A. van der Veen, P. C. J. Kamer and P. W. N. M. van Leeuwen, *Angew. Chem., Int. Ed.*, 1999, **38**, 336–338.

19 Y. Yan, X. Zhang and X. Zhang, *J. Am. Chem. Soc.*, 2006, **128**, 16058–16061.

20 A. M. Trzeciak, T. Głowiak, R. Grzybek and J. J. Ziółkowski, *J. Chem. Soc., Dalton Trans.*, 1997, 1831–1838.

21 M. Sparta, K. J. Børve and V. R. Jensen, *J. Am. Chem. Soc.*, 2007, **129**, 8487–8499.

22 D. Evans, J. A. Osborn and G. Wilkinson, *J. Chem. Soc. A*, 1968, 3133–3142.

23 M. R. Axet, S. Castillon and C. Claver, *Inorg. Chim. Acta*, 2006, **359**, 2973–2979.

24 P. C. J. Kamer, A. van Rooy, G. C. Schoemaker and P. W. N. M. van Leeuwen, *Coord. Chem. Rev.*, 2004, **248**, 2409–2424.

25 A. Aghmiz, C. Claver, A. M. Masdeu-Bultó, D. Maillard and D. Sinou, *J. Mol. Catal. A: Chem.*, 2004, **208**, 97–101.

26 T. Maji, C. H. Mendis, W. H. Thompson and J. A. Tunge, *J. Mol. Catal. A: Chem.*, 2016, **424**, 145–152.

27 C. Bianchini, H. M. Lee, A. Meli and F. Vizza, *Organometallics*, 2000, **19**, 849–853.

28 S.-I. Pien and S. S. C. Chuang, *J. Mol. Catal.*, 1991, **68**, 313–330.
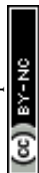
29 I. T. Horváth, R. V. Kastrup, A. A. Oswald and E. J. Mozeleski, *Catal. Lett.*, 1989, **2**, 85–90.

30 C. Kubis, M. Sawall, A. Block, K. Neymeyr, R. Ludwig, A. Börner and D. Selent, *Chem.–Eur. J.*, 2014, **20**, 11921–11931.

31 J. M. Dreimann, E. Kohls, H. F. W. Warmeling, M. Stein, L. F. Guo, M. Garland, T. N. Dinh and A. J. Vorholt, *ACS Catal.*, 2019, **9**, 4308–4319.

32 R. Whyman, K. A. Hunt, R. W. Page and S. Rigby, *J. Phys. E: Sci. Instrum.*, 1984, **17**, 559–561.

33 A. M. R. Hall, J. C. Chouler, A. Codina, P. T. Gierth, J. P. Lowe and U. Hintermair, *Catal. Sci. Technol.*, 2016, **6**, 8406–8417.

34 A. Martínez-Carrión, M. G. Howlett, C. Alamillo-Ferrer, A. D. Clayton, R. A. Bourne, A. Codina, A. Vidal-Ferran, R. W. Adams and J. Burés, *Angew. Chem., Int. Ed.*, 2019, **58**, 10189–10193.

35 A. C. Brezny and C. R. Landis, *ACS Catal.*, 2019, **9**, 2501–2513.

36 P. Suomalainen, H. K. Reinius, H. Riihimäki, R. H. Laitinen, S. Jääskeläinen, M. Haukka, J. T. Pursiainen, T. A. Pakkanen and A. O. I. Krause, *J. Mol. Catal. A: Chem.*, 2001, **169**, 67–78.

37 R. M. Deshpande, *Ind. Eng. Chem. Res.*, 1988, **27**, 1996.

38 E. Mieczyńska, A. M. Trzeciak and J. J. Ziółkowski, *J. Mol. Catal.*, 1992, **73**, 1–8.

39 B. E. Hanson and M. E. Davis, *J. Chem. Educ.*, 1987, **64**, 928.

40 M. Rosales, G. Chacón, A. González, I. Pacheco, P. J. Baricelli and L. G. Melean, *J. Mol. Catal. A: Chem.*, 2008, **287**, 110–114.

41 P. J. Baricelli, E. Lujano, M. Modroño, A. C. Marrero, Y. M. García, A. Fuentes and R. A. Sánchez-Delgado, *J. Organomet. Chem.*, 2004, **689**, 3782–3792.

42 D. B. G. Berry, A. Codina, I. Clegg, C. L. Lyall, J. P. Lowe and U. Hintermair, *Faraday Discuss.*, 2019, **220**, 45–57.

43 J. Y. Buser and A. D. McFarland, *Chem. Commun.*, 2014, **50**, 4234–4237.

44 J. M. Brown and A. G. Kent, *J. Chem. Soc., Perkin Trans. 2*, 1987, 1597–1607.

45 C. K. Brown and G. Wilkinson, *J. Chem. Soc. A*, 1970, 2753–2764.

46 R. F. Heck, *J. Am. Chem. Soc.*, 1968, **90**, 5518–5526.

47 I. S. Babra, L. S. Morley, S. C. Nyburg and A. W. Parkins, *J. Crystallogr. Spectrosc. Res.*, 1993, **23**, 997–1000.

48 R. V. Kastrup, J. S. Merola and A. A. Oswald, in *Catalytic Aspects of Metal Phosphine Complexes*, American Chemical Society, 1982, vol. 196, pp. 3–43.

49 L. A. van der Veen, M. D. K. Boele, F. R. Bregman, P. C. J. Kamer, P. W. N. M. van Leeuwen, K. Goubitz, J. Fraanje, H. Schenk and C. Bo, *J. Am. Chem. Soc.*, 1998, **120**, 11616–11626.

50 J. M. Brown, L. R. Canning, A. G. Kent and P. J. Sidebottom, *J. Chem. Soc., Chem. Commun.*, 1982, 721–723.

51 D. Evans, G. Yagupsky and G. Wilkinson, *J. Chem. Soc. A*, 1968, 2660–2665.

52 M. A. Freeman and D. A. Young, *Inorg. Chem.*, 1986, **25**, 1556–1560.

53 A. M. R. Hall, P. Dong, A. Codina, J. P. Lowe and U. Hintermair, *ACS Catal.*, 2019, **9**, 2079–2090.

54 G. J. H. Buisman, L. A. van der Veen, P. C. J. Kamer and P. W. N. M. van Leeuwen, *Organometallics*, 1997, **16**, 5681–5687.